

Unified representation of the C3, C4, and CAM photosynthetic pathways with the Photo3 model

Samantha Hartzell,^{1,2} Mark S. Bartlett,³ and Amilcare Porporato^{1,2*}

This is a preprint. The final, published version may be found in Ecological Modelling at <https://doi.org/10.1016/j.ecolmodel.2018.06.012> and may be cited as:

Hartzell S, Bartlett, M, Porporato A (2018) "Unified representation of the C3, C4, and CAM photosynthetic pathways with the Photo3 model" Ecological Modelling (384):173-187. DOI: 10.1016/j.ecolmodel.2018.06.012

*Corresponding Author: Amilcare Porporato
Department of Civil and Environmental Engineering
Princeton Environmental Institute
Princeton University
E-208 E-Quad, Princeton, NJ 08540 U.S.A.
Phone +1 609 258 2287
e-mail aporpora@princeton.edu

¹Department of Civil and Environmental Engineering, Princeton University

²Princeton Environmental Institute, Princeton University

³Department of Civil and Environmental Engineering, Duke University

Abstract

Recent interest in crassulacean acid metabolism (CAM) photosynthesis has resulted in new, physiologically based CAM models. These models show promise, yet unlike the more widely used physiological models of C3 and C4 photosynthesis, their complexity has thus far inhibited their adoption in the general community. Indeed, most efforts to assess the potential of CAM still rely on empirically based environmental productivity indices, which makes uniform comparisons between CAM and non-CAM species difficult. In order to represent C3, C4, and CAM photosynthesis in a consistent, physiologically based manner, we introduce the Photo3 model. Photo3 unites a common photosynthetic and hydraulic core with components depicting the circadian rhythm of CAM photosynthesis and the carbon-concentrating mechanism of C4 photosynthesis. This work allows consistent comparisons of the three photosynthetic types for the first time. It also allows the representation of intermediate C3-CAM behavior through the adjustment of a single model parameter. Model simulations of *Opuntia ficus-indica* (CAM), *Sorghum bicolor* (C4), and *Triticum aestivum* (C3) capture the diurnal behavior of each species as well as the cumulative effects of long-term water limitation. These results show the model's potential for evaluating the tradeoffs between C3, C4, and CAM photosynthesis, and for better understanding CAM productivity, ecology, and climate feedbacks.

Keywords

C3 photosynthesis · C4 photosynthesis · Crassulacean acid metabolism (CAM) · Plant water storage · Soil-plant-atmosphere continuum

1. Introduction

Crassulacean acid metabolism (CAM) and C4 photosynthesis are thought to have evolved as add-ons to the classical C3 photosynthetic pathway around 20-30 million years ago (Keeley and Rundel, 2003). Both photosynthetic processes achieve increased water use efficiency by concentrating CO₂ at the site of the dark reactions of photosynthesis. Today, C4 and CAM plants fill important ecological niches in grasslands, rainforests, and arid ecosystems; C4 plants dominate in grasslands where they account for almost 25% of terrestrial primary production (Still et al., 2003) whereas CAM plants make up almost 50% of plant biomass in certain arid and semi-arid regions of the world (Syvertsen et al., 1976). C4 crops such as corn (*Zea mays*), sugarcane (*Saccharum officinarum*), and sorghum (*Sorghum bicolor*) comprise 22% of the eighteen most common crops (Leff et al., 2004). CAM crops such as prickly pear (*Opuntia ficus indica*), agave (*Agave tequilana*), and pineapple (*Ananas comosus*) are also economically significant, particularly in arid and semi-arid regions of the world. Due to their extremely high water use efficiency and heat tolerance, the potential of CAM plants for food, fodder, and biofuel production will only become more significant as climate uncertainty and tensions over food scarcity increase (Nobel, 1991; García de Cortázar and Nobel, 1992; Borland et al., 2009; Owen and Griffiths, 2014; Mason et al., 2015).

Despite the prevalence and importance of CAM plants, physiological modeling of CAM photosynthesis is well behind that of C3 and C4 photosynthesis (Farquhar et al., 1980; Von Caemmerer and Furbank, 1999). Indeed, physiological models of CAM have only recently been introduced (see e.g. Owen and Griffiths (2013); Bartlett et al. (2014)) and have not been widely adopted. Instead, Nobel's Environmental Productivity Index (EPI), introduced in 1984, is the standard method of predicting net carbon uptake and yield for CAM plants (Nobel, 1988; Nair et al., 2012). This index, based on multiplicative indices for water, temperature and photosynthetically active radiation (PAR), is entirely empirical and does not

include a physiological representation of the CAM process. Furthermore, the index is designed to be calculated at a timescale of one month (Nobel, 1988; Owen and Griffiths, 2014), thus failing to take into account environmental variability at daily and weekly timescales, which has been shown to be an important factor in CAM functioning (Bartlett et al., 2014; Hartzell et al., 2015). This hampers the assessment of the potential impacts of CAM plants on climate, agriculture, and bioenergy production. Most climate modeling efforts include land surface models with a physiologically based representation of C3 (Rogers et al., 2017), and, often C4 photosynthesis (Cox, 2001; Cowling et al., 2007; Milly et al., 2014), but none currently include CAM photosynthesis, an important component of dryland and tropical ecosystems. The recent push for physiologically based crop modeling has also failed to take CAM crops into account. Multiple existing crop models, including 2Dleaf and MCWLA, are based on physiological models of C3 photosynthesis and stomatal conductance (Pachepsky and Acock, 1996; Tao et al., 2009), and the GECROS model supports both C3 and C4 photosynthesis based on modifications to the Farquhar model (Yin and Van Laar, 2005). Despite these advances, no crop models currently exist that are capable of coherently representing the three photosynthetic types. This discrepancy propagates into the analysis of bioenergy potential. While detailed biophysical models of C3 and C4 crops enable analyses of their potential for bioenergy production (Miguez et al., 2012; Nair et al., 2012), lack of detailed CAM modeling poses a problem in better understanding its potential in this area (Yan et al., 2011; Nair et al., 2012; Owen and Griffiths, 2014; Davis et al., 2015).

The Photo3 model addresses this need by providing a consistent, physiologically based description of CAM, C3, and C4 photosynthesis coupled to environmental conditions. The model seeks to balance the complexity required to faithfully represent each process with simplicity and clarity. To achieve this, the model leverages the commonalities between the three photosynthetic types. The core of the model is based on the Rubisco-mediated carbon assimilation achieved by the light reactions and Calvin cycle of C3 photosynthesis. When

representing CAM and C4 plants, this core is combined with a model for carbon fixation via phosphoenolpyruvate carboxylase (PEPC). The method for representing CAM plants is based on Bartlett et al. (2014), and adds a component for malic acid storage and release which is governed by an endogenous circadian rhythm. When representing C4 plants, a carbon concentrating mechanism based on Collatz et al. (1992); Von Caemmerer and Furbank (1999); Vico and Porporato (2008) is added to the model core. The resulting integrated model allows plants of all three photosynthetic types to be simulated on a consistent basis and in a wide variety of soil and atmospheric conditions.

In this work, the model is parameterized for one representative species from each photosynthetic type: *Opuntia ficus-indica* (CAM), *Triticum aestivum* (C3), and *Sorghum bicolor* (C4). Stomatal conductance, carbon assimilation, and water use of the three species are compared at the daily and monthly scale. Finally, intermediate C3-CAM behavior is explored through the adjustment of CAM model parameters. The Photo3 model accurately captures a wide range of photosynthetic behaviors and shows promise for applications in ecological, climate, and crop modeling. Written in Python, the model is open source and publicly available on GitHub. It employs a modular structure which allows it to be easily integrated with other routines for use in a variety of applications.

2. Materials and Methods

2.1. Overview of the Photo3 model

The core of the Photo3 model, given in Section 2.2, includes the Farquhar et al. (1980) model for photosynthetic demand, an optimal control model for stomatal conductance, and a model of the soil-plant-atmosphere continuum (SPAC). In the case of C4 and CAM photosynthesis, this core is coupled with a model for carbon fixation via PEPC, which is either spatially (C4) or temporally (CAM) separated from the Rubisco-mediated Calvin cycle. The SPAC model

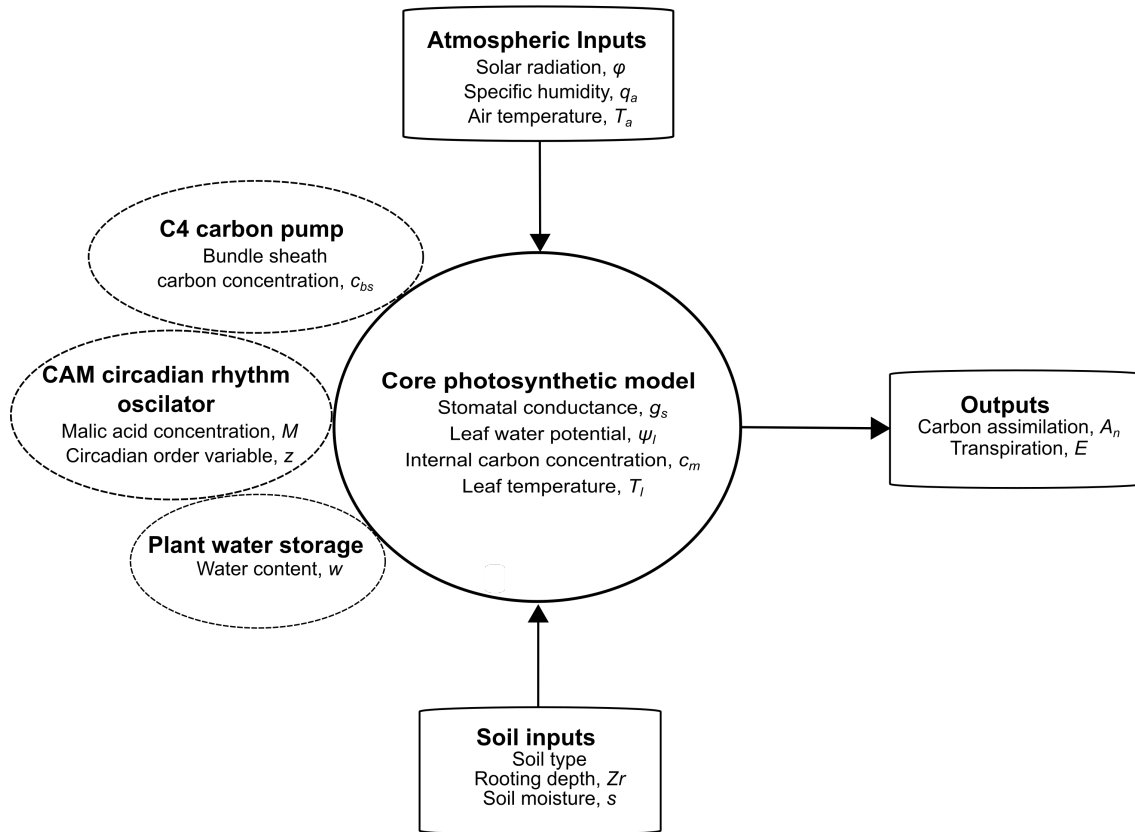


Figure 1: Photo3 model schematic. The Photo3 model is based on a core model of C3 photosynthesis with options to represent C4 photosynthesis, CAM photosynthesis, and plant water storage.

is a simple resistor-capacitor type model of the soil-plant-atmosphere continuum (e.g. Jones (1992)), and has an option to include plant water storage, which is an important feature in many succulent CAM species (Nobel, 1988). Given solar radiation, specific humidity, and temperature, the model estimates carbon assimilation and transpiration, as well as other variables of interest (see Figure 1).

The CAM model (formulated in Section 2.3) includes all of the features of the core model and adds a representation of the carbon concentrating mechanism. Based on Bartlett et al. (2014), the diurnal rhythm of malic acid production and release is modeled through the addition of a cell vacuole, characterized by M , the malic acid content, and z , the circadian order variable, which represents the overall effect of gene expression, enzyme activity and/or

the vacuole tonoplast in controlling the circadian rhythm. Depending on the values of M and z , CO_2 may either be fixed as malic acid by PEPC and later decarboxylated and released to the Calvin cycle, or it may be directly passed to the Calvin cycle and fixed via Rubisco. To account for the CAM idling process, dark respiration stays internal to the cell and is either passed to the cell vacuole or to the Calvin cycle, depending on the light level. These differences, described in Figure 2, allow the model to capture the unique diurnal rhythm of CAM carbon fluxes (Bartlett et al., 2014; Hartzell et al., 2015). Like the CAM model, the C4 model, presented in Section 2.4, also builds on the core Farquhar model. After the initial fixation of CO_2 into C4 acids via PEPC, which occurs in the mesophyll cell, the C4 acids are decarboxylated and the CO_2 is passed to the bundle sheath cell where it is concentrated. Within the bundle sheath cells, the Rubisco-mediated Calvin cycle fixes carbon into sugar (this process is represented using the Farquhar et al. (1980) model with the new, elevated CO_2 concentration c_{bs}). A graphical description of these carbon fluxes is given in Figure 2.

2.2. General photosynthetic relations

The net carbon uptake is modelled as a steady-state Fickian diffusion through the stomata, i.e.,

$$A_n = g_{s,\text{CO}_2}(c_s - c_m), \quad (1)$$

where g_{s,CO_2} is the stomatal conductance to CO_2 , c_s is the concentration of CO_2 at the leaf surface, and c_m is the concentration of CO_2 inside the mesophyll cytosol. The stomatal conductance is assumed to scale with the square root of the vapor pressure deficit following stomatal optimization theory, an approach which agrees well with accepted empirical models (Oren et al., 1999; Hari et al., 2000; Katul et al., 2009; Medlyn et al., 2011), and can be represented as

$$g_{s,\text{CO}_2} = \frac{a_1 A_n}{c_s \sqrt{D}}, \quad (2)$$

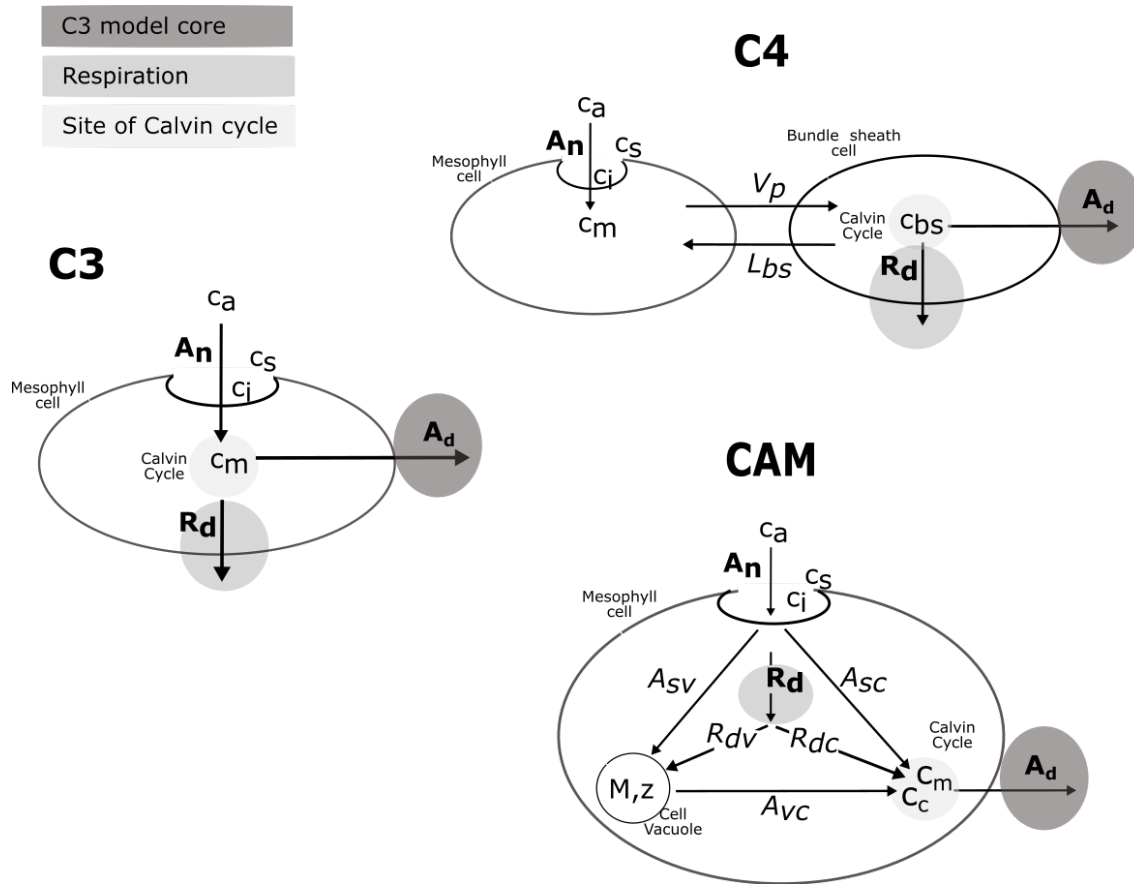


Figure 2: Representation of carbon fluxes. The C3, C4, and CAM photosynthesis models are based on a common photosynthetic core with additional fluxes to capture the spatial and temporal separations of CO₂ uptake and fixation.

where a_1 is an empirical constant which is adjusted to account for observed differences in the c_m/c_a ratio among photosynthetic types as described in Jones (1992) and D is the vapor pressure deficit.

The net photosynthetic demand for CO_2 , A_d , is modelled according to Farquhar et al. (1980) with an adjustment to account for plant water stress, i.e.,

$$A_d = A_{\phi, c_x, T_l}(\phi, c_x, T_l) \times f_{\psi_l}(\psi_l). \quad (3)$$

Due to the lack of temporal separation of CO_2 uptake and assimilation in C3 and C4 photosynthesis, the net carbon uptake A_n is equal to the net photosynthetic demand A_d for these photosynthetic types. The relationship between A_n and A_d for CAM includes a temporal separation and is described in Section 2.3. The carbon demand $A_{\phi, c_x, T_l}(\phi, c_x, T_l)$ is given by

$$A_{\phi, c_x, T_l}(\phi, c_x, T_l) = \min(A_c(c_x, T_l), A_q(\phi, c_x, T_l)), \quad (4)$$

where $A_c(c_x, T_l)$ is the Rubisco-limited photosynthetic rate, $A_q(\phi, c_x, T_l)$ is the light-limited photosynthetic rate, T_l is the leaf temperature, c_x is the CO_2 concentration at the site of the Calvin cycle, and ϕ is the incoming solar radiation (see Appendix A for details). The relevant CO_2 concentration c_x varies based on the photosynthetic type. For C3 plants, c_x is the mesophyll concentration c_m ; for C4 plants, it is the bundle sheath concentration c_{bs} ; and for CAM plants, it is either c_m or the corrected mesophyll CO_2 concentration c_c (when malic acid is being decarboxylated, the mesophyll CO_2 concentration is corrected to account for the elevated CO_2 concentration as $c_c = c_m(c_a, D) + c_o f_C(z, M)$ (Bartlett et al., 2014)).

The effects of water stress reduce the photosynthetic demand according to a ‘vulnerability’ function of the leaf water potential, $f_{\psi_l}(\psi_l)$, here represented for simplicity as a piecewise linear function which decreases between the point of onset of water stress, ψ_{lA1} , and the point

of stomatal closure ψ_{LA0} , i.e.,

$$f_{\psi_l}(\psi_l) = \begin{cases} 0, & \psi_l < \psi_{LA0} \\ \frac{(\psi_l - \psi_{LA0})}{(\psi_{LA1} - \psi_{LA0})}, & \psi_{LA0} < \psi_l \leq \psi_{LA1} \\ 1, & \psi_l > \psi_{LA1}, \end{cases} \quad (5)$$

where the leaf water potentials ψ_{LA1} and ψ_{LA0} are species-dependent (see Table 1). This piecewise function, also used in Daly et al. (2004), provides results similar to other response functions commonly used in describing plant response to water stress, such as sigmoidal curves (Sperry et al., 2002; Vico and Porporato, 2008), but has the advantage of providing increased numerical stability in the algorithm presented here, which involves solving relatively complex equations for the leaf water potential.

Since the dark respiration, R_d , is typically a small fraction of the carbon assimilation, its inclusion is optional except in the case of CAM where it is an important component of CAM idling behavior during periods of extended stomatal closure. Here it is represented as a temperature-dependent process according to a modified Arrhenius equation (see Appendix A).

2.3. CAM-specific relations

In the CAM model, a carbon pool is added to represent malic acid uptake and release from the cell vacuole (see Figure 2). The net flux of carbon through the stomata, A_n , is comprised of a flux from the stomata to the Calvin cycle, A_{sc} , and one to the cell vacuole, A_{sv} , i.e.,

$$A_n = A_{sc}(\phi, c_m, T_l, \psi_l, z, M) + A_{sv}(T_l, \psi_l, z, M), \quad (6)$$

where z and M are the circadian rhythm order variable and the malic acid concentration, respectively (described below), and the fluxes A_{sc} and A_{sv} are related to the carbon demand

A_d through the circadian state as described in Appendix C. The dark respiration flux, R_d , is likewise divided into a flux to the vacuole, R_{dv} , and one to the Calvin cycle, R_{dc} . Carbon is stored in the cell vacuole as malic acid and is released from the vacuole as the flux A_{vc} . The diurnal cycle of uptake and release from the vacuole, which governs the fluxes to and from the vacuole, is represented by a pair of balance equations for M , the malic acid concentration, and z , the circadian rhythm order. The balance equation for the malic acid concentration is given by

$$L_M \frac{dM}{dt} = A_{sv}(T_l, \psi_l, z, M) + R_{dv}(\phi, T_l) - A_{vc}(\phi, c_c, T_l, z, M), \quad (7)$$

where L_M is the ratio of malic acid storage volume to the carbon flux surface area, while the circadian rhythm order is given by

$$t_r \frac{dz}{dt} = \frac{M - M_E(z, T_l)}{M_{max}}, \quad (8)$$

where t_r is the relaxation time, M_E is the equilibrium concentration of malic acid, and M_{max} is the maximum malic acid concentration. The malic acid equilibrium concentration is given by

$$M_E(z, T_l) = \begin{cases} M_{max} \left[\left(\frac{T_H - T_l}{T_H - T_L} + 1 \right) c_1 [\beta(z - \mu)]^3 - \frac{T_H - T_l}{T_H - T_L} [\beta(z - \mu) - c_2] + [1 - f_0(z)] \right], & \phi \leq 0 \\ M_{max} \left[\left(\frac{T_H - T_l}{T_H - T_L} + 1 \right) c_1 [\beta(z - \mu)]^3 - \frac{T_H - T_l}{T_H - T_L} [\beta(z - \mu) - c_2] \right], & \phi > 0 \end{cases} \quad (9)$$

where T_H and T_L are the high and low temperature values for the circadian oscillation, and c_1 , c_2 , μ , and β are circadian oscillator constants included in Table 2. This formulation follows Bartlett et al. (2014) with the addition of the term $1 - f_0(z)$ which synchronizes the circadian rhythm with the prevailing light cycle (this new term increases M_E at high z values during the night, ensuring that the uptake of malic acid continues at night even if the previous day's cycle has not completely depleted the store of malic acid). The formulations

of the model fluxes are given in Appendix C. These adjustments to the functions given in Bartlett et al. (2014) improve model robustness to highly variable environmental inputs.

2.4. C4-specific relations

In the C4 plant, the influx of CO₂ to the bundle sheath cell is driven by the C4 pump and is modeled by a Michaelis-Menten type dependence on the mesophyll cytosol CO₂ concentration, c_m , as in Von Caemmerer (2000); Vico and Porporato (2008) (see Figure 2). The PEP regeneration rate, V_P , is bounded by the upper limit V_{Pr} , i.e.,

$$V_P(c_m) = \min \left(\frac{c_m V_{P,max}}{c_m + K_p}, V_{Pr} \right), \quad (10)$$

where $V_{P,max}$ is the maximum PEP carboxylation rate and K_p is the Michaelis-Menten coefficient. Leakage of CO₂ from the bundle sheath cell is modelled as a diffusion flux from the bundle sheath to the mesophyll cell, i.e.,

$$L_{bs}(c_{bs}, c_m) = g_{bs}(c_{bs} - c_m), \quad (11)$$

where g_{bs} is the conductance between the bundle sheath and mesophyll cells and c_{bs} is the CO₂ concentration in the bundle sheath cells. Finally, we introduce a balance equation for the CO₂ fluxes into and out of the bundle sheath cell, i.e.,

$$V_P(c_m) = A_d(\phi, c_{bs}, T_l, \psi_l) + L_{bs}(c_{bs}, c_m), \quad (12)$$

and solve for the CO₂ concentration in the bundle sheath cell, c_{bs} by combining Equation (12) with Equations (10) and (11). The carbon assimilation is then calculated according to Equation (3). Parameters for the C4 model are included in Table 3.

2.5. Plant hydraulics and capacitance

The transpiration flux, E , is driven by the difference between the specific humidity internal to the leaf and that of the atmosphere, i.e.,

$$E = g_{sa}\rho/\rho_w[q_i(T_l, \psi_l) - q_a], \quad (13)$$

where g_{sa} is the series of the atmospheric conductance and the combined stomatal-cuticular conductance (see Appendix B), ρ is the density of air, ρ_w is the density of water, q_i is the specific humidity internal to the leaf, and q_a is the specific humidity of the atmosphere. At the same time, the transpiration flux must be equal to the flux of water through the plant, i.e.,

$$E = g_{srp}(\psi_s - \psi_l), \quad (14)$$

where g_{srp} is the series of the soil-root and plant conductances (see Appendix B), ψ_s is the soil water potential, and ψ_l is the leaf water potential. These relations are joined by the equation for energy balance, which equates the incoming heat flux to the outgoing sensible and latent heat fluxes, i.e.,

$$\phi = g_a\rho c_p(T_l - T_a) + \lambda_w\rho_w E, \quad (15)$$

where ϕ is the incoming solar radiation, g_a is the atmospheric conductance, c_p is the specific heat of air, T_a is the atmospheric temperature, and λ_w is the latent heat of vaporization. Equations (13), (14) and (15) are solved simultaneously for the three unknowns: the transpiration E , the leaf temperature T_l , and the leaf water potential ψ_l .

Plant water storage is included as an option in the model. While it is generally negligible for most C3 and C4 crops, plant water storage significantly affects water stress and carbon assimilation for plants with a substantial water storage capacity, including most CAM plants.

Therefore, we include plant water storage when modeling CAM plants in this study, but not when modeling C3 and C4 plants. Plant water storage is represented in this model as a simple capacitor located at a height which is a fraction f of the total plant height as in Hartzell et al. (2017) (see Figure 3 and Appendix B). Using this scheme, the change in the plant relative water content w is given by the balance equation

$$LAI Z_w \frac{dw}{dt} = q_s(s, w) - E, \quad (16)$$

where Z_w is the total available water storage depth of the plant on a leaf area basis, LAI is the leaf area index, and s is the soil moisture. The transpiration flux E is now given by the sum of the fluxes from the soil, q_s , and the plant water storage, q_w , such that

$$E = q_s + q_w = g_{srpf}(\psi_s - \psi_x) + g_w LAI(\psi_w - \psi_x), \quad (17)$$

where ψ_x is the water potential at the storage connection node, g_{srpf} is the conductance between the soil and storage connection node, g_w is the conductance between the site of water storage and the storage connection node, and ψ_w is the water potential of the water storage tissue (see Appendix B and Table 4 for details). The addition of plant water storage adds a fourth unknown (ψ_x) to the water balance, which may now be formulated as described in Appendix B.

The soil moisture may either be provided as a model input or determined through the balance equation,

$$n Z_r \frac{ds}{dt} = -q_s(s, w) - L(s) - E_v(s) + R(t), \quad (18)$$

where n is the soil porosity, Z_r is the rooting depth and s is the volumetric soil moisture averaged over the rooting depth. Total losses from the soil are due to plant water uptake $q_s(s, w)$, leakage loss $L(s)$, and evaporation $E_v(s)$ (see Rodriguez-Iturbe and Porporato

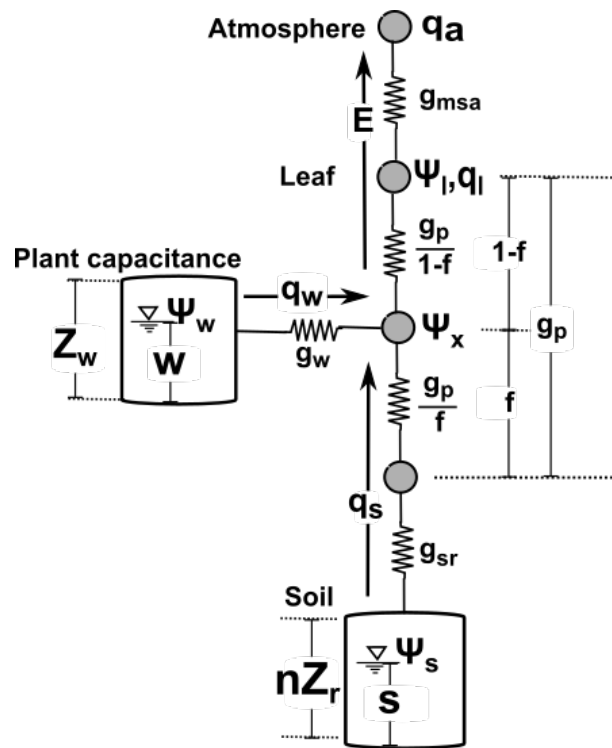


Figure 3: Representation of hydraulic fluxes. The involved hydraulic fluxes are calculated using a resistor-capacitor model of the soil-plant-atmosphere continuum with optional plant water storage.

(2004) for details). In Equation (18), the rainfall $R(t)$ may be specified either as a model input or may be generated within the model as a stochastic process which requires the mean rainfall depth and frequency as input parameters. Currently a range of soil types are represented by the four soil options included in the model: loamy sand, sandy loam, loam, and clay. Soil parameters are included in Table 5.

2.6. Model Implementation

The model requires inputs of environmental conditions including solar radiation, air temperature, specific humidity, soil moisture, and soil type. Because of the strong dependence of CAM photosynthesis on variability in environmental conditions at the sub-daily scale, the model operates with a 30-minute timestep. Solar radiation, specific humidity, and air temperature data with an hourly timescale may be interpolated to give values at each model timestep. Alternatively, values for these variables may be generated internally to the model using a built-in boundary-layer simulation following the approach presented in Daly et al. (2004). The model is currently parameterized with hydraulic and photosynthetic properties for three representative species, *Triticum aestivum* (C3), *Sorghum bicolor* (C4), and *Opuntia ficus-indica* (CAM) (see Tables 1, 3, 2, and 4); these species were selected because they are among the most well-studied and economically important species of each photosynthetic group (Leff et al., 2004; Paterson et al., 2008). These properties are meant to represent plants at the mature stage in the growing season, and are assumed to be approximately constant over the model duration.

2.7. Model validation and testing

2.7.1. Model validation

The model was validated using data collected under both well-watered and droughted conditions for the three representative crops (see Section 3.1). Model results under well-watered conditions for *Opuntia ficus-indica* were compared to results from a 24-hour laboratory experiment undertaken by Nobel and Hartsock (1983) with 12 hours of light and 12 hours of darkness. In this simulation, the day period was characterized by a solar radiation of 244 W/m^2 , a temperature of 25 C, and a relative humidity of 40%, while the night period was characterized by a temperature of 15 C and a relative humidity of 60% according to the conditions present in the laboratory experiment. To facilitate comparisons of model performance with experimental data for *S. bicolor* and *T. aestivum*, the model was forced with typical non-limiting laboratory conditions of 12 h light:12 h darkness with a photosynthetic photon flux density (PPFD) of 1800 $\mu mol/m^2/s$ during the light period, a constant temperature of 26 C, constant relative humidity of 80%, and 0.7 volumetric soil moisture in loam soil. To enable comparison of model results with data for *O. ficus-indica*, the model was run for a 40 day drydown in loamy sand with solar radiation, temperature, and relative humidity obtained from the National Solar Radiation Database (NSRDB) (National Renewable Energy Laboratory, 2017) on March 17, 2015 at a weather station nearby the study location in Til Til, Chile. Results were compared with data from Acevedo et al. (1983) describing carbon assimilation and stomatal conductance of under water-stressed conditions,

2.7.2. Diurnal dynamics

The diurnal dynamics of the three photosynthetic types were compared under typical, well-watered, growing conditions (see Section 3.2). The model was run using meteorological data from Temple, TX on April 1, 2015, imposing a soil moisture of 0.5 and a soil type of sandy

loam. The solar radiation, air temperature, and specific humidity for the site were obtained from the NSRDB data viewer (National Renewable Energy Laboratory, 2017).

2.7.3. Long-term performance under drought

We evaluated the relative long-term performance of the three crops during a drought (Section 3.3) by simulating a drydown of 40 days was simulated beginning with a volumetric soil moisture of 0.5 and using temperature, relative humidity, and solar radiation data from Temple TX from April 1, 2015 until May 10, 2015 (National Renewable Energy Laboratory, 2017). During the drydown, the soil moisture was calculated according to Eq. (18).

2.7.4. Representation of C3-CAM intermediates

To test the ability of the model to capture C3/CAM intermediate photosynthetic types, the model was executed with various levels of maximum malic acid storage capacity, M_{max} (see Section 3.4). Values tested were $M_{max} = 190 \text{ mol/m}^3$ (default model setting), 95 mol/m^3 (50% of the default setting), and 1.9 mol/m^3 (1% of the default setting). Results from these simulations were compared to a simulation run with all the photosynthetic parameters of *O. ficus-indica*, but with the photosynthetic type set equal to C3 rather than CAM. In each of these simulations, plant water storage and respiration were not included. Simulations were run for sandy loam soil with a constant soil moisture of 0.5 and weather conditions found in Temple, TX on April 3, 2015 (National Renewable Energy Laboratory, 2017).

3. Results and discussion

3.1. Model validation

For *O. ficus-indica*, the magnitude and diurnal dynamics of both carbon assimilation (see Figure 4a) and stomatal conductance (data not shown) closely match those observed in

controlled laboratory experiments. Carbon assimilation reaches a maximal value of $10 \mu\text{mol}/\text{m}^2/\text{s}$, in agreement with the data, and stomatal conductance reaches a maximal value of $3.0 \text{ mm}/\text{s}$, as compared with the observed maximal value of $2.8 \text{ mm}/\text{s}$. The diurnal dynamics show a relatively good fit, with a slight underestimate of carbon assimilation in the middle of the night (hours 21-1) and a slight overestimate of carbon assimilation at dawn (hour 6). At dusk, the timing of the onset of CAM carbon assimilation matches very well with the data, while the decrease in carbon assimilation and stomatal conductance at dawn is slightly slower than that observed. For *S. bicolor*, the carbon assimilation rate under optimal conditions is $48 \mu\text{mol}/\text{m}^2/\text{s}$, which lies within the range of published experimental ranges of $34\text{-}48 \mu\text{mol}/\text{m}^2/\text{s}$ (Peng, 1990) and $40 \mu\text{mol}/\text{m}^2/\text{s}$ (Resende et al., 2012) (see Figure 4c). For *T. aestivum*, the maximal simulated carbon assimilation rate is $28 \mu\text{mol}/\text{m}^2/\text{s}$, which agrees well with experimental values of $24\text{-}29 \mu\text{mol}/\text{m}^2/\text{s}$ (Evans, 1983) and $32 \mu\text{mol}/\text{m}^2/\text{s}$ (Martin and Ruiz-Torres, 1992) (see Figure 4e).

Model responses to water limitations also compare well with data for the three representative species. Figure 4b shows daily maximal stomatal conductance for *O. ficus-indica* at various levels of soil water potential simulated during a drydown. The daily maximal stomatal conductance decreases from a maximum under well-watered conditions to 50% of its original value at a soil water potential of approximately -0.7 MPa . This behavior is a good fit with field measurements of stomatal conductance taken during a progressive drydown (Acevedo et al., 1983). Finally, the model response to water limitation $f_{\psi_l}(\psi_l)$, given by Equation (5), is compared with experimental data for carbon assimilation at a range of leaf water potentials for both *S. bicolor* and *T. aestivum*. Data shown include two cultivars of *S. bicolor*: ICSV 1063 and MIGSOR (data from Contour-Ansel et al. (1996)), and several cultivars of *T. aestivum*: Kanchan, Sonalika, Kalyansona, and C306 (data from Siddique et al. (2000)), TAM W-101 (data from (Johnson et al., 1987)), and TAM W-101 and Sturdy (data from (Martin and Ruiz-Torres, 1992)) (see Figure 4d, f). The response of the model

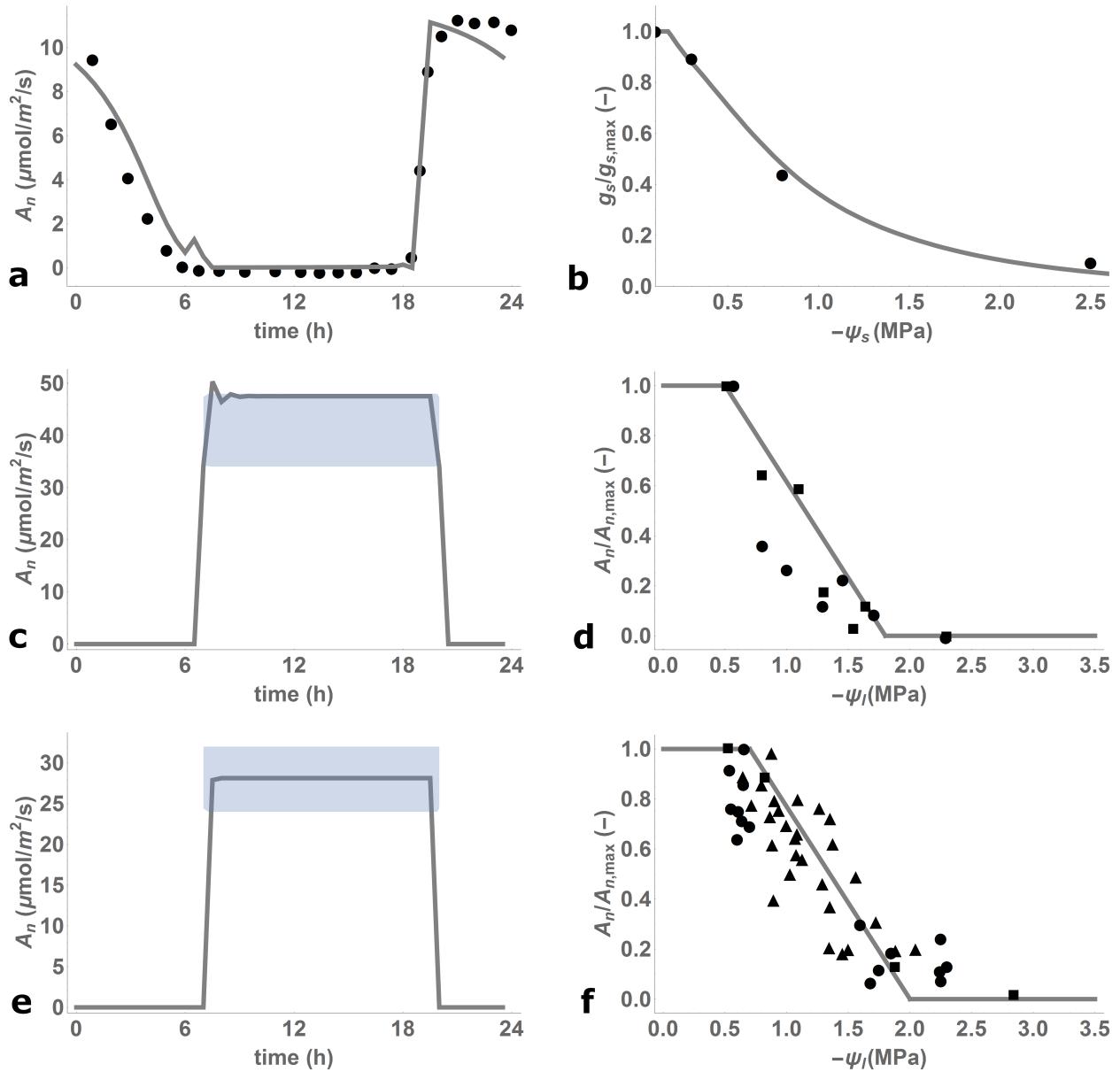


Figure 4: Comparison with experimental data. (a) Comparison of modeled carbon assimilation, A_n ($\mu\text{mol}/\text{m}^2/\text{s}$) for *Opuntia ficus-indica* (solid line) with data from Nobel and Hartsock (1983) (circles). (b) Comparison of modeled decrease in stomatal conductance g_s as a fraction of maximal stomatal conductance $g_{s,max}$ for *O. ficus-indica* during a drydown period with data from Acevedo et al. (1983) (circles). (c) Comparison of modeled carbon assimilation as a function of maximal carbon assimilation, $A_{n,max}$, for *Sorghum bicolor* with published ranges in laboratory experiments according to Peng (1990); Resende et al. (2012) (gray shading). (d) Comparison of modeled decrease in carbon assimilation with leaf water potential for *S. bicolor* and data from Contour-Ansel et al. (1996) for two cultivars: ICSV 1063 (circles) and MIGSOR (squares). (e) Comparison of modeled carbon assimilation for *Triticum aestivum* with published ranges in laboratory experiments according to Evans (1983); Martin and Ruiz-Torres (1992) (gray shading). (f) Comparison of modeled decrease in carbon assimilation with leaf water potential and data for four cultivars of *T. aestivum* (Kanchan, Sonalika, Kalyansona, and C306) from Siddique et al. (2000) (circles), data for TAM W-101 (Johnson et al., 1987) (squares), and data for TAM W-101 and Sturdy (Martin and Ruiz-Torres, 1992) (triangles).

to moisture limitations generally agrees with published data for these species and provides a fit similar to that obtained through a sigmoidal function of leaf water potential.

3.2. Diurnal dynamics

Due to its detailed representation of CAM dynamics, the Photo3 model is able to compare CAM, C3, and C4 functioning at a half-hourly timescale. Figure 5a shows the solar radiation, air temperature, and specific humidity for a typical April day in Temple, TX. Model responses of carbon assimilation, transpiration, and stomatal conductance for each of the photosynthetic types are shown in Figure 5b-d. The characteristic stomatal behavior of CAM is clearly shown, with stomata opening primarily at night. A combination of a low stomatal conductance and a low nocturnal driving force for transpiration during this period result in a very low transpiration with a moderate nocturnal carbon assimilation. The carbon concentrating behavior of C4 results in a high maximum carbon assimilation, while the stomatal conductance and transpiration are slightly lower than that of C3. Under these conditions, the C4 plant shows a high productivity and a high water use efficiency, while the CAM plant shows a relatively low productivity but a very high water use efficiency.

3.3. Long-term performance under drought

Model simulations of cumulative carbon assimilation and water use during a drought period are shown in Figure 6 for the three photosynthetic types. While the C3 and C4 crops initially have high productivity, assimilating carbon at a rate two to three times that of the CAM crop, the productivity of the C3 and C4 crops undergoes a large decrease after about 8-10 days as the soil dries to below 0.3 volumetric soil moisture (Figure 6a). Meanwhile, the CAM crop exhibits a slower, but more persistent rate of carbon gain. By day 22, the total carbon assimilation of *O. ficus-indica* surpasses that of *T. aestivum*, and by day 29, it surpasses

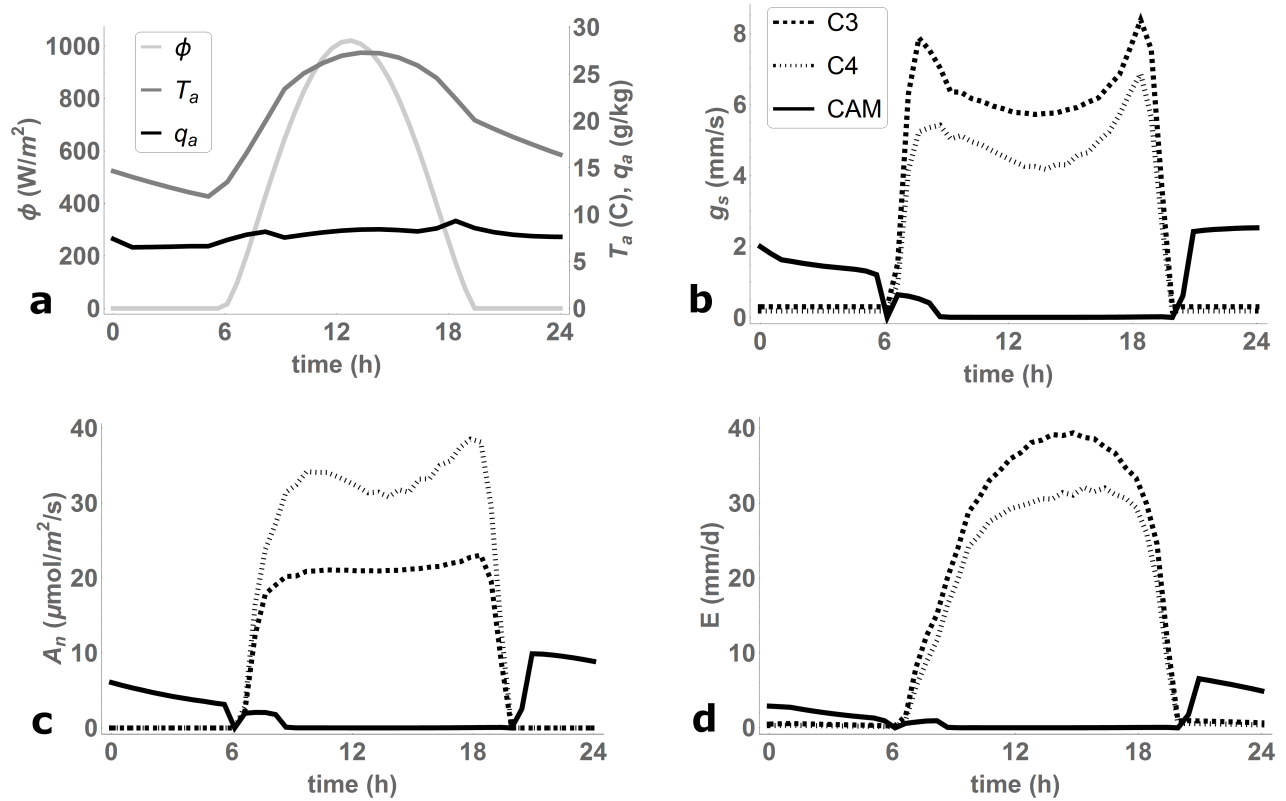


Figure 5: A comparison of the diurnal behavior of the three photosynthetic types. (a) Model inputs of solar radiation ϕ (W/m^2), temperature T (C) and specific humidity q_a (g/kg) obtained using data from Temple, TX on April 30, 2015. (b) Simulated stomatal conductance to water vapor g_s (mm/s) on a leaf area basis, (c) simulated carbon assimilation A_n ($\mu\text{mol}/\text{m}^2/\text{s}$) on a leaf area basis, and (d) simulated transpiration E (mm/d) on a ground area basis for *Triticum aestivum* (C3), *Sorghum bicolor* (C4), and *Opuntia ficus-indica* (CAM) under non-water-limited conditions (soil moisture of 0.5).

that of *S. bicolor*. The CAM crop also shows a much lower cumulative transpiration, by a factor of nearly five, during the early stages of the drought, while the overall water use of the C3 and C4 crops are similar during this period (see Figure 6b). This allows the soil moisture in the CAM simulation to remain at a much higher level for the first 20 days of the simulation (see Figure 6c). While the CAM species exhibits a lower productivity under non-water-limited conditions, it exhibits a much higher water use efficiency and its productivity persists longer under water-limited conditions. After a 40-day drydown, the CAM crop ultimately assimilates twice as much carbon as the C3 species and 50% more than the C4 species. At the same time, its total transpiration is less than half that of the C3 species and about 70% that of the C4 species. Depending on the specific environmental conditions, the photosynthetic water use efficiency of CAM is two to six times higher than C3, and one to five times higher than C4 (Figure 6d). This consistent basis of comparison, which incorporates the effects of environmental variability at both long and short timescales, allows the model user to quantify the costs and benefits of crops with different photosynthetic types in water-limited ecosystems.

3.4. Representation of C3-CAM intermediates

CAM photosynthesis is generally not a discrete trait, rather, a spectrum of C3-CAM behavior exists in nature (Winter et al., 2015; Bräutigam et al., 2017). Metabolite fluxes similar to CAM fluxes have been shown in C3 plants, to a much smaller degree (Winter et al., 2015; Bräutigam et al., 2017), and some cacti, including *O. ficus-indica*, *Agave deserti*, and *Mesembryanthemum crystallinum* show dramatic changes in the level of CAM expression throughout their lifespan, switching from C3 to CAM photosynthesis during the process of development or in response to water stress (Kluge and Ting, 1978; Winter et al., 1978; Jordan and Nobel, 1979; Acevedo et al., 1983; Winter et al., 2008; Winter and Holtum, 2011). The consistent formulations of the three different photosynthetic pathways in the Photo3 model

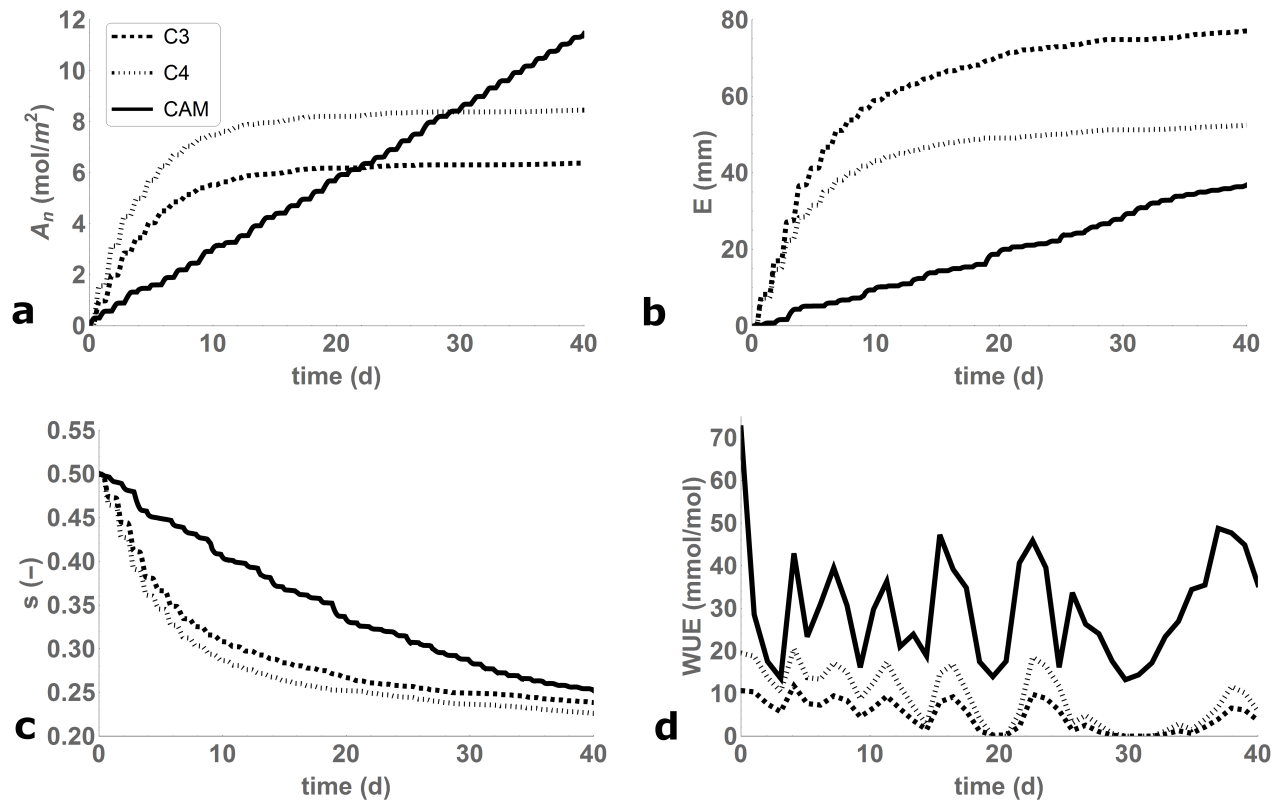


Figure 6: A comparison of the long-term performance under drought for the three photosynthetic types. Simulated (a) cumulative carbon assimilation A_n (mol/m²) on a leaf area basis, (b) cumulative transpiration E (mm) on a leaf area basis, (c) volumetric soil moisture s , and (d) instantaneous water-use efficiency WUE (mmol/mol) over the course of 40 days beginning on April 1, 2015 in Temple, TX.

allows intermediate CAM-C3 behavior to be explored through the adjustment of a single model parameter. This is the first time that such an analysis has been possible in a model coupled to the soil-plant-atmosphere continuum.

As CAM expression becomes stronger, vacuole size and maximum malic acid storage capacity increase. Indeed, maximum malic acid content is a typical measure of the strength of CAM expression (Kluge and Ting, 1978). By altering the maximum malic acid concentration M_{max} in the CAM model, C3 behavior can be retrieved from the CAM model framework. These results are shown in Figure 7a-c, which shows carbon assimilation, transpiration, and stomatal conductance for *O. ficus-indica* with varying degrees of malic acid storage capacity (full CAM expression with 100% malic acid storage capacity, CAM intermediate with 50% malic acid storage capacity, and CAM intermediate with 1% malic acid storage capacity), and with C3 type photosynthesis. As the maximum malic acid concentration approaches zero, the length of nocturnal stomatal opening becomes shorter until it approaches zero in accordance with the C3 model. Meanwhile, the stomata begin to open for increasingly longer periods during the day. For very low values of maximum malic acid concentration, the stomatal conductance, carbon assimilation, and transpiration of the CAM model match those of the C3 model.

The relevant CAM fluxes A_{sv} , A_{vc} , and A_{sc} are shown in Figure 7d-f for various levels of CAM expression. As M_{max} decreases, the fluxes A_{sv} and A_{vc} decrease, while the duration of A_{sc} increases until it is occurring for all daylight hours as M_{max} approaches zero. This behavior can be understood by referring to Appendix C. As M_{max} decreases, the amount of malic acid stored during the night becomes smaller, and the malic acid is more quickly depleted during the day. As a result, the carbon function f_C , which depends on the malic acid concentration (see Equation (C.3)) is at a non-zero value for a briefer period after the onset of light. As f_C approaches zero during the day, A_{vc} approaches zero and A_{sc} approaches A_n , yielding C3-like behavior (see Equations (C.9) and (C.1)). Likewise, the flux

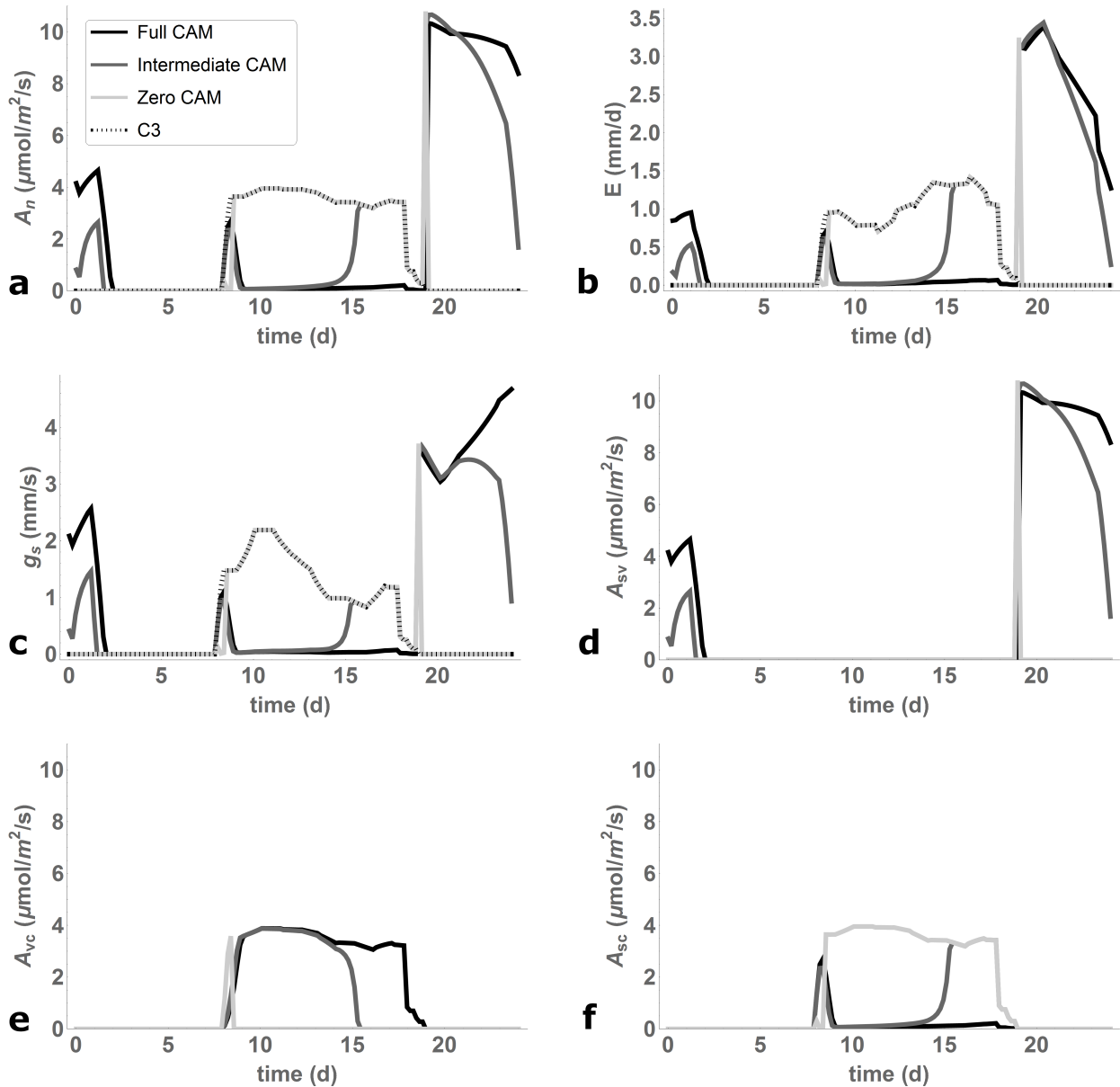


Figure 7: Simulation of CAM-C3 intermediates. (a-c) Comparison of CAM-C3 intermediates with C3 photosynthesis. Simulated (a) carbon assimilation A_n ($\mu\text{mol}/\text{m}^2/\text{s}$) on a leaf area basis, (b) transpiration E (mm/d) on a ground area basis, and (c) stomatal conductance g_s (mm/s) to water vapor on a leaf area basis. (d-f) Carbon fluxes for CAM-C3 intermediates. Fluxes (d) A_{sv} from the stomata to the vacuole, (e) A_{vc} from the vacuole to the Calvin cycle, and (f) A_{sc} from the stomata to the Calvin cycle. All simulations are based on parameters for *Opuntia ficus-indica* with a constant soil moisture of 0.5 and weather conditions found in Temple, TX on April 3, 2015.

A_{sv} is restricted to smaller time increments at dawn and dusk and finally approaches zero according to Equation (C.5).

4. Conclusions

Results of the Photo3 model allow the comparison of CAM, C3, and C4 species in a consistent framework. This detailed model is streamlined, user-friendly, and robust to a wide range of environmental conditions. Thus, it is ready to be included as a component of earth system models, crop models, and bioenergy models. In each of these areas, a more detailed representation of CAM functioning can illuminate important questions. The inclusion of C4 plants in earth system models has been evaluated and has been shown to have a significant effect on land cover and on local climate conditions (Cowling et al., 2007). Thus, CAM plants, which arguably inhabit more extreme climates, may also be expected to show important local effects. A more detailed representation of CAM in crop modeling will be a useful tool for evaluating potential productivity, planting strategies, and water use strategies for CAM agriculture. The open source, modular nature of the Photo3 model allows for the addition of other features that may help to explore a wide range of research questions. In this stage of its development, Photo3 currently assumes static plant traits like leaf area index, root area index, and photosynthetic capacity, and outputs plant water use and carbon assimilation as a function of climate conditions. In the future, additional modules may be added to support the inclusion of more inputs, such as plant nutrient status and growing stage, and outputs like biomass accumulation and crop yield. As pressure increases to provide food, water, and energy to a growing population, ecohydrological modeling tools such as Photo3 will be necessary to quantitatively evaluate the tradeoffs between species with different photosynthetic strategies (Porporato et al., 2015).

The Photo3 model, for the first time, provides a physiologically based and consistent rep-

resentation of the three photosynthetic types (CAM, C3, and C4) coupled to environmental conditions. This is done using a consistent model core built on the Farquhar et al. (1980) model for carbon assimilation, a model of stomatal functioning based on stomatal optimality, and a resistor-capacitor model of the soil-plant-atmosphere continuum. The model allows the user to compare expected productivity and water use efficiency of CAM plants directly with that of C3 and C4 plants under a wide range of climate conditions. The results produced here for simulations of *Opuntia ficus-indica*, *Triticum aestivum*, and *Sorghum bicolor*, show detailed predictions of stomatal conductance, carbon assimilation, and transpiration at the daily level and also facilitate the comparison of long-term carbon assimilation and water use of the three photosynthetic types under drought conditions. Through the adjustment of a single model parameter, the model framework is also able to capture intermediate C3-CAM behavior. The open source, modular nature of the model is designed for to be user friendly and easy to couple with existing modeling efforts. Photo3 shows promise for use in a variety of research applications where models of CAM photosynthesis are currently lacking, including the prediction of CAM climate feedbacks, productivity, and biofuel potential.

Software availability

The Photo3 software can be accessed for free at <https://samhartz.github.io/Photo3/>. It was created by Samantha Hartzell, Mark Bartlett, and Amilcare Porporato (email aporporo@princeton.edu, phone 609 258 2287), and first made available in 2017. Photo3 was developed in Python 2.7 with the SciPy, NumPy, Pandas, Tkinter, and Matplotlib packages. Program size is 45.6 KB. We suggest installing a Python distribution such as Anaconda to meet the program requirements.

Acknowledgements

This work was supported through the USDA Agricultural Research Service cooperative agreement 58-6408-3-027 and National Institute of Food and Agriculture (NIFA) grant 12110061; and National Science Foundation (NSF) grants CBET-1033467, EAR-1331846, FESD-1338694, EAR-1316258, GRFP-1106401 and the Duke WISeNet Grant DGE-1068871. We thank Marina Smalling for her useful feedback.

Appendix

A. Details of the general photosynthetic model

The Rubisco-limited rate of carbon assimilation, A_c , is given by

$$A_c(c_x, T_l) = V_{c,max} \frac{c_x - \Gamma^*(T_l)}{c_x + K_c(T_l)(1 + o_i/K_o(T_l))}, \quad (\text{A.1})$$

where $V_{c,max}$ is the maximum carboxylation rate, c_x is the relevant CO₂ concentration (see Equation (4)), K_c and K_o are the Michaelis-Menten coefficients for CO₂ and O₂, respectively, o_i is the oxygen concentration, and Γ^* is the CO₂ compensation point (see Table 1 for the model parameters). The maximum carboxylation rate, $V_{c,max}$, and the CO₂ compensation point, Γ^* , are given by

$$V_{c,max}(T_l) = V_{c,max0} \frac{\exp[\frac{H_{aJ}}{RT_0}(1 - \frac{T_0}{T_l})]}{1 + \exp(\frac{S_{vC}T_l - H_{dL}}{RT_l})} \quad (\text{A.2})$$

and

$$\Gamma^*(T_l) = \Gamma_0[1 + \Gamma_1(T_l - T_0) + \Gamma_2(T_l - T_0)^2], \quad (\text{A.3})$$

where R is the universal gas constant (J/(mol K)), T_0 is a reference temperature, and the remaining parameters are given in Table 1. The temperature dependence of the Michaelis-

Menten constants K_c and K_o is described by a modified Arrhenius equation, i.e.,

$$K_x(T_l) = K_{x0} \exp \left[\frac{H_{Kx}}{RT_0} \left(1 - \frac{T_0}{T_l} \right) \right]. \quad (\text{A.4})$$

The light-limited assimilation rate, A_q , is given by

$$A_q(\phi, c_x, T_l) = \frac{J(\phi, T_l)}{4} \frac{(c_x - \Gamma^*(T_l))}{(c_x + 2\Gamma^*(T_l))}, \quad (\text{A.5})$$

where J , the electron transport rate, is equal to $\min(J_{max}(T_l), J_\phi(\phi))$. The maximum potential electron transport rate, $J_{max}(T_l)$, is given by

$$J_{max}(T_l) = J_{max0} \frac{\exp\left[\frac{H_{aJ}}{RT_0} \left(1 - \frac{T_0}{T_l}\right)\right]}{1 + \exp\left(\frac{S_{vQ}T_l - H_{aJ}}{RT_l}\right)}, \quad (\text{A.6})$$

while the PAR limited electron transport rate, $J_\phi(\phi)$, is given by

$$J_\phi(\phi) = \frac{\phi \lambda \kappa_2}{2N_a h c}, \quad (\text{A.7})$$

where ϕ is the incoming radiation (W/m^2), 50 percent of which is considered photosynthetically active radiation (PAR) (Jones, 1992), λ is the average wavelength (m) for PAR (assumed to be 550 nm), h is Planck's constant (Js), c is the speed of light (m/s), N_a is Avogadro's constant (mol^{-1}), and κ_2 is the quantum yield of photosynthesis in $\text{mol CO}_2 \text{ mol}^{-1}$ photons.

The dark respiration R_d is modelled according to an identical Arrhenius equation with coefficients R_{d0} and H_{kR} (see Leuning (1995); Bartlett et al. (2014)).

B. Details of the hydraulic model

Water potentials

The soil water potential, ψ_s , is related to the soil moisture through a strongly nonlinear function given by Rodriguez-Iturbe and Porporato (2004) and Daly et al. (2004) as

$$\psi_s(s) = \bar{\psi}_s s^{-b}, \quad (\text{B.1})$$

where $\bar{\psi}_s$ is the soil water potential at saturation and b is the exponent of the retention curve. The specific plant water capacitance c , is defined as the change in relative stored water volume per unit change in water potential ($c = dw/d\psi_w$). In this study we have chosen to approximate the plant water capacitance as constant and the stored water potential ψ_w as a linear function of the relative water storage volume w following Hunt et al. (1991), i.e.,

$$\psi_w(w) = \frac{w - 1}{c}. \quad (\text{B.2})$$

This relationship neglects nonlinearities in the pressure-volume relationship caused by osmotic effects at low w in order to include plant water storage with a minimum level of complexity. Although a simplification, this linear relationship is a good approximation in the physically relevant regime for many succulent and CAM species (Nobel and Jordan, 1983; Hunt and Nobel, 1987; Ogburn and Edwards, 2012). In *O. ficus-indica* specifically, the pressure-volume relationship has been shown to be approximately linear for relative water contents above 20%; below this point further decreases in relative water content will lead to tissue damage and are not considered reversible (Goldstein et al., 1991).

Conductances

The stomatal conductance to water, g_{s,H_2O} , is closely related to the stomatal conductance for CO₂ given in Equation (2) and is here given by

$$g_{s,H_2O} = 1.6g_{s,CO_2} + g_{cut}, \quad (\text{B.3})$$

where the factor 1.6 accounts for the differences between the the diffusivity in air of CO₂ and H₂O (Jones, 1992). The cuticular conductance, g_{cut} , is added to the stomatal conductance to account for the small amount of water vapor lost in the absence of carbon assimilation (Burghardt and Riederer, 2003).

Following Daly et al. (2004), the soil-root conductance, g_{sr} , is assumed to be proportional to the soil hydraulic conductivity, $K(s)$, divided by the average distance from the soil to root surface, i.e.,

$$g_{sr}(s) = \frac{K(s)\sqrt{RAI_w s^{-d}}}{\pi g \rho_w Z_r}, \quad (\text{B.4})$$

where RAI_w is the root area index under well-watered conditions, s^{-d} is a term introduced to model root growth under water-stressed conditions, g is the gravitational constant, and Z_r is the rooting depth. The hydraulic conductivity $K(s)$ is given by

$$K(s) = K_s s^{2b+3}, \quad (\text{B.5})$$

where K_s is the saturated hydraulic conductivity and b is a parameter defined in Equation (B.1) (see Table 5).

The decrease in plant conductance under water stress is modeled by a vulnerability curve so that g_p is close to g_{pmax} for high ψ_l and is close to 0 for low ψ_l due to xylem cavitation

(Sperry et al., 1998; Daly et al., 2004), i.e.,

$$g_p = g_{pmax} \exp \left[- \left(\frac{-\psi_l}{j} \right)^h \right]. \quad (\text{B.6})$$

where h and j are shape parameters. Following Waring and Running (1978) and Carlson and Lynn (1991), the conductance between the water storage tissue and the xylem is assumed to decrease with the fraction of stored water following a power law given by

$$g_w = g_{wmax} w^m, \quad (\text{B.7})$$

where g_{wmax} is the maximum storage-xylem conductance and a is a parameter between 1 and 10, here assumed to be equal to 4. Due to the linear relationship between w and ψ_w imposed by Equation (B.2), this assumption is equivalent to assuming a power law relationship between the stored water potential ψ_w and the conductance g_p .

Hydrology balance with plant water storage

In the absence of plant water storage, the hydrology balance may be described through Equations (13), (14), and (15), which are solved simultaneously for the leaf water potential, ψ_l , the leaf temperature, T_l , and the transpiration E . When plant water storage is included, the formulation of hydrology balance is slightly altered, and a fourth variable, ψ_x , is introduced, which describes the water potential at the storage connection node. Equation (14) is now given by

$$E = \frac{g_p}{1-f} (\psi_x - \psi_l), \quad (\text{B.8})$$

where $\frac{g_p}{1-f}$ is the hydraulic conductance between the storage connection node and the leaf (see Figure 3). Now the hydraulic balance is described by Equations (13), (15), (17), and (B.8). To solve this system of equations, Equation (B.8) is solved for ψ_x and substituted

into Equation (17), eliminating the unknown ψ_x , i.e.

$$E = \frac{g_{srfp}(\psi_s - \psi_l) + LAI g_w(\psi_w - \psi_l)}{1 + \frac{g_{srfp}(1-f)}{LAI g_p} + \frac{g_w(1-f)}{g_p}}. \quad (\text{B.9})$$

The resulting system of three equations - Equation (13), (15), and (B.9) - is now solved simultaneously for the three unknowns, ψ_l , T_l , and E .

C. Details of the CAM photosynthetic model

The CAM photosynthetic fluxes A_{sc} , A_{sv} , A_{vc} are modified from Bartlett et al. (2014) to improve model robustness to a range of environmental conditions. The flux A_{sc} from the stomata to the Calvin cycle is given by

$$A_{sc}(\phi, c_m, T_l, \phi_l, z, M) = \max[(A_{\phi, c_m, T_l}(\phi, c_m, T_l) - R_{dc}(T_l)) \times f_{\psi_l}(\psi_l) \times (1 - f_C(z, M)), 0], \quad (\text{C.1})$$

where $R_{dc}(T_l)$ is the respiration flux to the Calvin cycle and is given by

$$R_{dc}(T_l) = R_d(T_l)(1 - \exp(\phi)). \quad (\text{C.2})$$

The carbon function $f_C(z, M)$ accounts for the circadian rhythm control of the flux dictated by the values of M and z and is given by

$$f_C(z, M) = (1 - f_O(z)) \frac{M}{\alpha_1 M_{max} + M}, \quad (\text{C.3})$$

where the order function $f_O(z)$ describes the relative rate of malic acid diffusion from the cell vacuole to the cytoplasm and the overall activation state of the decarboxylation enzymes and is given by

$$f_O(z) = \exp \left[- \left(\frac{z}{\mu} \right)^{c_3} \right], \quad (\text{C.4})$$

where μ and c_3 are circadian oscillator constants given in Table 2. Note that for $f_C = 0$ the flux A_{sc} is the same as the C3 carbon assimilation given in Equation (3).

The flux A_{sv} from the stomata to the vacuole is adjusted from Bartlett et al. (2014) with a modification which prevents the flux from occurring when light is present and the vacuole is empty. The modified flux is given by

$$A_{sv}(T_l, \psi_l, z, M) = \begin{cases} 0, & \phi > 0 \text{ \& } M \ll 1 \\ (A_{sv,max}(T_l) - R_{dv}(T_l)) \times f_{\psi_l}(\psi_l) \times f_M(z, M, T_l), & \textit{otherwise}, \end{cases} \quad (\text{C.5})$$

where the malic acid storage function $f_M(z, M, T_l)$ accounts for the circadian control of the flux and is given by

$$f_M(z, M, T_l) = f_O(z) \frac{M_S(T_l) - M}{\alpha_2 M_S(T_l) + (M_S(T_l) - M)}, \quad (\text{C.6})$$

where $M_S(T_l)$ is the maximum storage concentration of malic acid and is given by

$$M_S(T_l) = M_{max} \left[\frac{T_H - T_l}{T_H - T_L} (1 - \alpha_2) + \alpha_2 \right], \quad (\text{C.7})$$

where T_H and T_L are the high and low temperature bounds of the circadian rhythm and α_2 is a parameter of the circadian oscillator. $R_{dv}(T_l)$ is the respiration flux to the cell vacuole, given by

$$R_{dv}(T_l) = R_d(T_l) \exp(-\phi). \quad (\text{C.8})$$

Finally, the flux A_{vc} from the vacuole to the Calvin cycle is given by

$$A_{vc}(\phi, c_c, T_l, z, M) = (A_{\phi,c_c,T_l} - R_{dc}(T_l)) \times f_C(z, M). \quad (\text{C.9})$$

Table 1: Plant Photosynthetic Parameters

Parameter	<i>O. ficus-indica</i>	<i>S. bicolor</i>	<i>T. aestivum</i>	Units	Description
a_1	2.08 ^{a, b}	1.73 ^{a, b}	3.46 ^a		Stomatal conductance coefficient, Eq. (2)
K_{c0}	302 ^a	302	302	$\mu\text{mol mol}^{-1}$	Michaelis constant for CO ₂ at T_o
K_{o0}	256 ^a	256	256	mmol mol^{-1}	Michaelis constant for O ₂ at T_o
H_{kc}	59430 ^a	59430	59430	J mol^{-1}	Activation energy for Kc
H_{ko}	36000 ^a	36000	36000	J mol^{-1}	Activation energy for Ko
R_{d0}	0.32 ^a	0.32	4.93 ^c	$\mu\text{mol m}^{-2} \text{s}^{-1}$	Standard dark respiration at 25 C
H_{kR}	53000 ^a	53000	53000	J mol^{-1}	Activation energy for Rd
κ_2	0.3 ^d	0.3	0.3	$\text{mol CO}_2 \text{ mol}^{-1} \text{ photons}$	Quantum yield of photosynthesis, Eq. (A.7)
$V_{c,max0}$	13 ^e	39 ^f	107.4 ^c	$\mu\text{mol m}^{-2} \text{s}^{-1}$	Maximum carboxylation rate
H_{aV}	72000 ^g	72000	62000	J mol^{-1}	Activation energy for $V_{c,max}$
H_{dV}	200000 ^g	200000 ^h	202900 ^h	J mol^{-1}	Deactivation energy for $V_{c,max}$
J_{max0}	26 ⁱ	180 ^f	184.9 ^c	$\mu\text{mol m}^{-2} \text{s}^{-1}$	Electron transport rate, Eq. (A.6)
H_{aJ}	50000 ^g	50000	50000	J mol^{-1}	Activation energy for J_{max}
H_{dJ}	200000 ^g	200000	200000	J mol^{-1}	Deactivation Energy for J_{max}
o_i	0.209 ^a	0.209	0.209	mol mol^{-1}	Oxygen concentration
S_{vC}	649 ^g	649	649	J mol^{-1}	Entropy term for carboxylation
S_{vQ}	646 ^g	646	646	J mol^{-1}	Entropy term for electron transport
T_o	293.2 ^a	293.2	293.2	K	Reference temperature
Γ_o	34.6 ^a	34.6	34.6	$\mu\text{mol mol}^{-1}$	CO ₂ compensation point at T_o , Eq. (A.3)
Γ_1	0.0451 ^a	0.0451	0.0451	K^{-1}	Eq. (A.3)
Γ_2	0.000347 ^a	0.000347	0.000347	K^{-2}	Eq. (A.3)
ψ_{lA1}	-0.5 ^j	-0.5 ^k	-0.7 ^l	MPa	Onset of plant water stress, Eq. (5)
ψ_{lAO}	-3 ^j	-1.8 ^k	-2 ^l	MPa	Point of maximum plant water stress, Eq. (5)

^a Based on Leuning (1995)

^b Based on Jones (1992)

^c Based on Sun et al. (2015)

^d Based on Long et al. (1993)

^e Based on Nobel and Hartssock (1983); Cui et al. (1993); Pimienta-Barrios et al. (2000)

^f Based on Collatz et al. (1992)

^g Based on Kattge and Knorr (2007)

^h Based on Daly et al. (2004)

ⁱ Twice $V_{c,max}$, as suggested by Kattge and Knorr (2007)

^j Based on Bartlett et al. (2014)

^k Based on Contour-Ansel et al. (1996)

^l Based on Siddique et al. (2000)

Table 2: CAM photosynthetic parameters (based on *Opuntia ficus-indica*)

Constant	Value	Units	Description
c_1	0.365 ^a		Circadian oscillator constant
c_2	0.55 ^a		Circadian oscillator constant
c_3	10 ^a		Circadian oscillator constant
μ	0.5 ^a		Circadian oscillator constant
β	2.764 ^a		Circadian oscillator constant
M_{max}	190 ^a	mol m ⁻³	Maximum malic acid concentration
$A_{m,max}$	13.5 ^a	$\mu\text{mol m}^{-2}\text{s}^{-1}$	Maximum rate of malic acid storage flux
t_r	90 ^a	min	Relaxation time
α_1	1/100 ^a		
α_2	1/7 ^a		
k	0.003 ^a		
T_{opt}	288.65 ^a	K	
T_H	302.65 ^a	K	High temperature
T_L	283.15 ^a	K	Low temperature
c_o	3000 ^a	$\mu\text{mol mol}^{-1}$	Parameter for decarboxylation of malic acid

^a Based on (Bartlett et al., 2014).

^b Empirical constant added to increase model robustness

Table 3: C4 Photosynthetic Parameters (based on *Sorghum bicolor*)

Parameter	Value	Units	Description
g_{bs}	.013 ^a	mol m ⁻² s ⁻¹	Conductance between bundle sheath and mesophyll
$V_{P,max}$	120 ^b	$\mu\text{mol/m}^{-2}\text{s}^{-1}$	Maximum PEP carboxylation rate
V_{pr}	80 ^c	$\mu\text{mol/m}^{-2}\text{s}^{-1}$	PEP regeneration rate
K_p	80 ^c	$\mu\text{mol mol}^{-1}$	Michaelis-Menten coefficient for C4

^a Based on Vico and Porporato (2008)

^b Based on (Jones, 1992; Vico and Porporato, 2008)

^c Based on (Von Caemmerer, 2000; Vico and Porporato, 2008)

Table 4: Plant Hydraulic Parameters

Parameter	<i>O. ficus-indica</i>	<i>S. bicolor</i>	<i>T. aestivum</i>	Units	Description
g_{pmax}	0.04 ^a	0.13 ⁱ	11.7 ^d	$\mu\text{m MPa}^{-1} \text{s}^{-1}$	Maximum xylem conductance per unit leaf area
LAI	3 ^b	5 ^j	5 ^o	$\text{m}^2 \text{m}^{-2}$	Leaf area per unit ground area
Z_r	0.1 ^c	0.5 ^k	0.75 ^p	m	Mean rooting depth
RAI_w	3 ^c	5.6 ^l	5.6 ^l	$\text{m}^2 \text{m}^{-2}$	Root area index under well watered conditions
d	8 ^d	8 ^d	8 ^d		Parameter accounting for root growth
α_m	1 ^e	2.65 ^l	1.65 ^l	$\text{mol m}^{-2} \text{s}^{-1}$	Ratio of $g_{m,CO2}$ to $g_{s,CO2}$
g_{cut}	0 ^b	0.1802 ^m	0.3 ^q	mm s^{-1}	Cuticular conductance per unit leaf area
g_a	324 ^f	61 ⁿ	61 ⁿ	mm s^{-1}	Atmospheric conductance per unit ground area
Z_w	0.00415 ^g	-	-	$\text{m}^3 \text{m}^{-2}$	Maximum depth of water stored per unit leaf area
g_{wmax}	0.002 ^a	-	-	$\mu\text{m MPa}^{-1} \text{s}^{-1}$	Maximum conductance between stored water and transport
h	2 ^d	-	-		Parameter for Eq. (B.6)
j	2 ^d	-	-		Parameter for Eq. (B.6)
m	4 ^h	-	-		Parameter for Eq. (B.7)
c	0.27 ^g	-	-	MPa^{-1}	Intrinsic plant hydraulic capacitance, Eq. (B.2)
f	0.5	-	-		Fractional height of hydraulic capacitance

^a Estimated from a succulent CAM species based on Bartlett et al. (2014)

^b Based on Nobel (1988)

^c Based on Snyman (2005)

^d Based on Daly et al. (2004)

^e Based on Flexas et al. (2008)

^f Based on Jones (1992) for a windspeed of 2 m/s at 2 m altitude, with a plant height of 2 m.

^g Based on Goldstein et al. (1991)

^h Based on values from Waring and Running (1978); Carlson and Lynn (1991)

ⁱ Based on Kocacinar and Sage (2003)

^j Based on Olufayo et al. (1996)

^k Based on Bremner et al. (1986)

^l Based on Vico and Porporato (2008)

^m Based on Muchow and Sinclair (1989)

ⁿ Based on Jones (1992) for a windspeed of 2 m/s at 2 m altitude, with a plant height of 1 m.

^o Based on Lunagaria and Shekh (2006)

^p Based on Bandyopadhyay et al. (2003)

^q Based on Kerstiens (1996)

Table 5: Soil Parameters

Parameter	Loamy sand	Sandy loam	Loam	Clay
K_s (cm d ⁻¹)	100	80	20	1
$\bar{\psi}_s$ (MPa)	$-1.7 \cdot 10^{-4}$	$-7.0 \cdot 10^{-4}$	$-1.43 \cdot 10^{-3}$	$-1.82 \cdot 10^{-3}$
b	4.38	4.9	5.39	11.4
n	0.42	0.43	0.45	0.5
s_h	0.08	0.14	0.19	0.47

^a Parameters from Rodriguez-Iturbe and Porporato (2004)

References

- Acevedo E, Badilla I, Nobel PS (1983) Water Relations, Diurnal Acidity Changes, and Productivity of a Cultivated Cactus, *Opuntia ficus-indica*. *Plant Physiology* 72(3):775–780
- Bandyopadhyay PK, Mallick S, Rana SK (2003) Actual evapotranspiration and crop coefficients of onion (*Allium cepa* L.) under varying soil moisture levels in the humid tropics of India. *Tropical Agriculture* 80(2):83–90
- Bartlett MS, Vico G, Porporato A (2014) Coupled carbon and water fluxes in CAM photosynthesis: modeling quantification of water use efficiency and productivity. *Plant and Soil* 383(1-2):111–138
- Borland AM, Griffiths H, Hartwell J, Smith JaC (2009) Exploiting the potential of plants with crassulacean acid metabolism for bioenergy production on marginal lands. *Journal of Experimental Botany* 60(10):2879–2896
- Bräutigam A, Schlüter U, Eisenhut M, Gowik U (2017) On the Evolutionary Origin of CAM Photosynthesis. *Plant physiology* 174:473–477
- Bremner P, Preston G, Fazekas C, de St CG (1986) A field comparison of sunflower (*Helianthus annuus*) and sorghum (*Sorghum bicolor*) in a long drying cycle. I. Water extraction. *Crop and Pasture Science* 37(5)
- Burghardt M, Riederer M (2003) Ecophysiological relevance of cuticular transpiration of deciduous and evergreen plants in relation to stomatal closure and leaf water potential. *Journal of experimental botany* 54(389):1941–9
- Carlson T, Lynn B (1991) The effects of plant water storage on transpiration and radiometric surface temperature. *Agricultural and forest meteorology* 57(1986)

- Collatz GJ, Ribas-Carbo M, Berry Ja (1992) Coupled photosynthesis-stomatal conductance model for leaves of C4 plants. *Australian Journal of Plant Physiology* 19(1139):519–539
- Contour-Ansel D, Ilami G, Ouarzane A, Louguet P (1996) Effect of water stress on pyruvate, Pi dikinase and phosphoenol pyruvate carboxylase activities in the leaves of two cultivars of sorghum (*sorghum bicolor* L.). *Journal of Agronomy and Crop Science* 176:59–69
- Cowling SA, Jones CD, Cox PM (2007) Consequences of the evolution of C4 photosynthesis for surface energy and water exchange. *Journal of Geophysical Research* 112
- Cox PM (2001) Description of the “TRIFFID” Dynamic Global Vegetation Model. Hadley Centre technical note
- Cui M, Miller PM, Nobel PS (1993) CO₂ Exchange and Growth of the Crassulacean Acid Metabolism Plant *Opuntia ficus-indica* under Elevated CO₂ in Open-Top Chambers. *Plant Physiology* 103(2):519–524
- Daly E, Porporato A, Rodriguez-Iturbe I (2004) Coupled Dynamics of Photosynthesis, Transpiration, and Soil Water Balance. Part I: Upscaling from Hourly to Daily Level. *Journal of Hydrometeorology* 5(3):546–558
- Davis SC, Davis SC, Ming R, Lebauer DS, Long SP (2015) Toward systems-level analysis of agricultural production from crassulacean acid metabolism (CAM): scaling from cell to commercial production. *New Phytologist* 208:66–72
- Evans JR (1983) Nitrogen and Photosynthesis in the Flag Leaf of Wheat (*Triticum aestivum* L.). *Plant Physiology* 72(2):297–302
- Farquhar G, Caemmerer SV, Berry J (1980) A biochemical model of photosynthetic CO₂ assimilation in leaves of C3 species. *Planta* 149:78–90

- Flexas J, Ribas-Carbó M, Diaz-Espejo A, Galmés J, Medrano H (2008) Mesophyll conductance to CO₂: Current knowledge and future prospects. *Plant, Cell and Environment* 31(5):602–621
- García de Cortázar V, Nobel PS (1992) Biomass and Fruit Production for the Prickly Pear Cactus , *Opuntia ficus-indica*. *J Amer Soc Hort Sci* 117(4):558–562
- Goldstein G, Andrade JL, Nobel PS (1991) Differences in water relations parameters for the chlorenchyma and the parenchyma of *Opuntia ficus-indica* under wet versus dry conditions. *Australian Journal of Plant Physiology* 18(2):95–107
- Hari P, Mäkelä A, Pohja T (2000) Surprising implications of the optimality hypothesis of stomatal regulation gain support in a field test. *Australian Journal of Plant Physiology* 27:77–80
- Hartzell S, Bartlett MS, Virgin L, Porporato A (2015) Nonlinear dynamics of the CAM circadian rhythm in response to environmental forcing. *Journal of Theoretical Biology* 368:83–94
- Hartzell S, Bartlett MS, Porporato A (2017) The role of plant water storage and hydraulic strategies in relation to soil moisture availability. *Plant and Soil* 419(1-2):503–521
- Hunt E, Nobel P (1987) Non-Steady-State Water Flow for Three Desert Perennials With Different Capacitances. *Australian Journal of Plant Physiology* 14(4):363
- Hunt RE, Running SW, Federer C (1991) Extrapolating plant water flow resistances and capacitances to regional scales. *Agricultural and Forest Meteorology* 54(24):169–195
- Johnson RC, Mornhinweg DW, Ferris DM, Heitholt JJ (1987) Leaf photosynthesis and conductance of selected triticum species at different water potentials. *Plant physiology* 83(4):1014–7

- Jones H (1992) *Plants and microclimate: a quantitative approach to environmental plant physiology*. Cambridge University Press
- Jordan PW, Nobel S (1979) Infrequent Establishment of Seedlings of *Agave deserti* (Agavaceae) in the Northwestern Sonoran Desert. *American Journal of Botany* 66(9):1079–1084
- Kattge J, Knorr W (2007) Temperature acclimation in a biochemical model of photosynthesis: a reanalysis of data from 36 species. *Plant, cell & environment* 30(9):1176–90
- Katul GG, Palmroth S, Oren RAM (2009) Leaf stomatal responses to vapour pressure deficit under current and CO₂-enriched atmosphere explained by the economics of gas exchange. *Plant Cell and Environment* 32:968–979
- Keeley JE, Rundel PW (2003) Evolution of CAM and C₄ Carbon Concentrating Mechanisms. *International Journal of Plant Sciences* 164(S3):55–77
- Kerstiens G (1996) Cuticular water permeability and its physiological significance. *Journal of Experimental Botany* 47(305):1813–1832
- Kluge M, Ting IP (1978) *Crassulacean Acid Metabolism: Analysis of an Ecological Adaptation*. Springer-Verlag, New York
- Kocacinar F, Sage RF (2003) Photosynthetic pathway alters xylem structure and hydraulic function in herbaceous plants. *Plant, Cell and Environment* 26(12):2015–2026
- Leff B, Ramankutty N, Foley JA (2004) Geographic distribution of major crops across the world. *Global Biogeochemical Cycles* 18(1)
- Leuning R (1995) A critical appraisal of a combined stomatal-photosynthesis model for C₃ plants

- Long SP, Postl WF, Bolhár-Nordenkampf HR (1993) Quantum yields for uptake of carbon dioxide in C3 vascular plants of contrasting habitats and taxonomic groupings. *Planta* 189(2):226–234
- Lunagaria MM, Shekh AM (2006) Radiation interception, light extinction coefficient and leaf area index of wheat (*Triticum aestivum* L.) crop as influenced by row orientation and row spacing. *Journal of Agricultural Sciences* 2(2):43–54
- Martin B, Ruiz-Torres Na (1992) Effects of Water-Deficit Stress on Photosynthesis, Its Components and Component Limitations, and on Water Use Efficiency in Wheat (*Triticum aestivum* L.). *Plant physiology* 100(2):733–739
- Mason PM, Glover K, Smith JAC, Willis KJ, Woods J, Thompson IP (2015) The potential of CAM crops as a globally significant bioenergy resource: moving from fuel or food’ to fuel and more food’. *Energy Environ Sci* 8:2320–2329
- Medlyn BE, Duursma RA, Eamus D, Ellsworth DS, Barton CV, Crous KY, Angelis PD, Freeman M, Wingate L (2011) Reconciling the optimal and empirical approaches to modelling stomatal conductance. *Global Change Biology* 17(6):2134–2144
- Miguez FE, Maughan M, Bollero GA, Long SP (2012) Modeling spatial and dynamic variation in growth, yield, and yield stability of the bioenergy crops *Miscanthus giganteus* and *Panicum virgatum* across the conterminous United States. *GCB Bioenergy* 4(5):509–520
- Milly PCD, Malyshev SL, Shevliakova E, Dunne KA, Findell KL, Gleeson T, Liang Z, Phillips P, Stouffer RJ, Swenson S (2014) An Enhanced Model of Land Water and Energy for Global Hydrologic and Earth-System Studies. *Journal of Hydrometeorology* 15(4):1739–1761
- Muchow RC, Sinclair TR (1989) Epidermal conductance, stomatal density and stomatal size

- among genotypes of *Sorghum bicolor* (L.) Moench. *Plant, Cell & Environment* 12(4):425–431
- Nair SS, Kang S, Zhang X (2012) Bioenergy crop models: descriptions, data requirements, and future challenges. *GCB Bioenergy* 4:620–633
- National Renewable Energy Laboratory (2017) NSDRB Data Viewer
- Nobel PS (1988) *Environmental biology of agaves and cacti*. Cambridge University Press, Cambridge
- Nobel PS (1991) Achievable productivities of certain CAM plants: basis for high values compared with C3 and C4 plants. *New Phytologist* 119(2):183–205
- Nobel PS, Hartsock TL (1983) Relationships between Photosynthetically Active Radiation, Nocturnal Acid Accumulation, and CO₂ Uptake for a Crassulacean Acid Metabolism Plant, *Opuntia ficus-indica*. *Plant physiology* 71(1):71–75
- Nobel PS, Jordan PW (1983) Transpiration stream of desert species: resistances and capacitances for a C3, a C4 and a CAM plant. *Journal of Experimental Botany* 34(147):1379–1391
- Ogburn RM, Edwards EJ (2012) Quantifying succulence: a rapid, physiologically meaningful metric of plant water storage. *Plant, cell & environment* 35(9):1533–42
- Olufayo A, Baldy C, Ruelle P (1996) Sorghum yield, water use and canopy temperatures under different levels of irrigation. *Agricultural Water Management* 30(1):77–90
- Oren R, Sperry JS, Katul GG, Pataki DE, Ewers BE, Phillips N, Schäfer KVR (1999) Survey and synthesis of intra- and interspecific variation in stomatal sensitivity to vapour pressure deficit. *Plant, Cell & Environment* 22(12):1515–1526

- Owen N, Griffiths H (2013) A system dynamics model integrating physiology and biochemical regulation predicts extent of crassulacean acid metabolism (CAM) phases. *New Phytologist* 200(4):1116–1131
- Owen NA, Griffiths H (2014) Marginal land bioethanol yield potential of four crassulacean acid metabolism candidates (*Agave fourcroydes*, *Agave salmiana*, *Agave tequilana* and *Opuntia ficus-indica*) in Australia. *GCB Bioenergy* 6(6):687–703
- Pachepsky LB, Acock B (1996) A model 2DLEAF of leaf gas exchange: Development, validation, and ecological application. *Ecological Modelling* 93(1-3):1–18
- Paterson AH, Felker P, Hubbell SP, Ming R (2008) The Fruits of Tropical Plant Genomics. *Tropical plant biology* 1(1):3–19
- Peng S (1990) Gas exchange and water use efficiency of grain sorghum. PhD thesis
- Pimienta-Barrios E, Zañudo J, Yopez E, Pimienta-Barrios E, Nobel PS (2000) Seasonal variation of net CO₂ uptake for cactus pear (*Opuntia ficus-indica*) and pitayo (*Stenocereus queretaroensis*) in a semi-arid environment. *Journal of Arid Environments* 44(1):73–83
- Porporato A, Feng X, Manzoni S, Mau Y, Parolari AJ, Vico G (2015) Ecohydrological modeling in agroecosystems: Examples and challenges. *Water Resources Research* 6(4):446
- Resende RS, Rodrigues FÁ, Cavatte PC, Martins SCV, Moreira WR, Chaves ARM, Damatta FM (2012) Leaf gas exchange and oxidative stress in sorghum plants supplied with silicon and infected by *Colletotrichum sublineolum*. *Phytopathology* 102(9):892–8
- Rodriguez-Iturbe I, Porporato A (2004) *Ecohydrology of water-controlled ecosystems*. Cambridge University Press

- Rogers A, Medlyn B, Dukes J, Bonan G, Caemmerer S, Dietze M, Kattge J, Leakey A, Mercado L, Niinemets Ü, Prentice I (2017) A roadmap for improving the representation of photosynthesis in Earth system models. *New Phytologist* 213(1)
- Siddique MRB, Hamid A, Islam M (2000) Drought stress effects on water relations of wheat. *Botanical Bulletin of Academia Sinica* 41
- Snyman H (2005) A case study on in situ rooting profiles and Water-Use Efficiency of cactus pears, *Opuntia ficus-indica* and *O. robusta*. *Journal for the professional association for cactus development* 7:1–21
- Sperry J, Hacke U, Oren R, Comstock J (2002) Water deficits and hydraulic limits to leaf water supply. *Plant Cell and Environment* 25(2):251–263
- Sperry JS, Adler FR, Campbell GS, Comstock JP (1998) Limitation of plant water use by rhizosphere and xylem conductance: Results from a model. *Plant, Cell and Environment* 21(4):347–359
- Still CJ, Berry JA, Collatz GJ, Defries RS (2003) Global distribution of C3 and C4 vegetation: Carbon cycle implications. *Global Biogeochemical Cycles* 17(1)
- Sun J, Sun J, Feng Z (2015) Modelling photosynthesis in flag leaves of winter wheat (*Triticum aestivum*) considering the variation in photosynthesis parameters during development. *Functional Plant Biology* 42(11):1036–1044
- Syvertsen JP, Nickell GL, Spellenberg RW, Cunningham GL (1976) Carbon reduction pathways and standing crop in three Chihuahuan desert plant communities. *Southwestern Naturalist* 21(3)(3):311–320
- Tao F, Yokozawa M, Zhang Z (2009) Modelling the impacts of weather and climate variability on crop productivity over a large area: A new process-based model development,

- optimization, and uncertainties analysis. *Agricultural and Forest Meteorology* 149(5):831–850
- Vico G, Porporato A (2008) Modelling C3 and C4 photosynthesis under water-stressed conditions. *Plant and Soil* 313(1-2):187–203
- Von Caemmerer S (2000) *Biochemical models of leaf photosynthesis*. CSIRO publishing
- Von Caemmerer S, Furbank R (1999) Modeling C4 Photosynthesis. In: Sage R, Monson R (eds) *C4 plant biology*, Academic Press, New York, pp 173–211
- Waring R, Running S (1978) Sapwood water storage: its contribution to transpiration and effect upon water conductance through the stems of old growth Douglas fir. *Plant, Cell & Environment* 1(2):131–140
- Winter K, Holtum JAM (2011) Induction and reversal of crassulacean acid metabolism in *Calandrinia polyandra*: effects of soil moisture and nutrients. *Functional Plant Biology* 38:576–582
- Winter K, Lüttge U, Winter E (1978) *Oecologia to Crassulacean Acid Metabolism in Its Natural Environment*. *Oecologia* 237:225–237
- Winter K, Garcia M, Holtum JAM (2008) On the nature of facultative and constitutive CAM : environmental and developmental control of CAM expression during early growth of *Clusia* , *Kalanchoe*, and *Opuntia*. *Journal of Experimental Botany* 59(7):1829–1840
- Winter K, Holtum JAM, Smith JAC (2015) Crassulacean acid metabolism: a continuous or discrete trait? *New Phytologist* 208:73–78
- Yan X, Tan DKY, Inderwildi OR, Smith JAC, King DA (2011) Life cycle energy and greenhouse gas analysis for agave-derived bioethanol. *Energy & Environmental Science* 4(9):3110

Yin X, Van Laar H (2005) Crop Systems Dynamics: An ecophysiological simulation model for genotype-by-environment interactions. Wageningen Academic Pub